BIOCHEMISTRY
including biophysical chemistry & molecular biology

Article

pubs.acs.org/biochemistry

Component Interactions and Electron Transfer in Toluene/*o*-Xylene Monooxygenase

Alexandria Deliz Liang and Stephen J. Lippard*

Department of Chemistry, Massachusetts Institute of Technology, Cambridge, Massachusetts 02139, United States

Supporting Information

ABSTRACT: The multicomponent protein toluene/*o*-xylene monooxygenase (ToMO) activates molecular oxygen to oxidize aromatic hydrocarbons. Prior to dioxygen activation, two electrons are injected into each of two diiron(III) units of the hydroxylase, a process that involves three redox active proteins: the ToMO hydroxylase (ToMOH), Rieske protein (ToMOC), and an NADH oxidoreductase (ToMOF). In addition to these three proteins, a small regulatory protein is essential for catalysis (ToMOD). Through steady state and pre-steady state kinetics studies, we show that ToMOD attenuates electron transfer from ToMOC to ToMOH in a concentration-dependent manner. At substoichiometric concentrations, ToMOD increases the rate of turnover, which we interpret to be a consequence of opening a pathway for oxygen transport to the catalytic diiron center in ToMOH. Excess ToMOD inhibits steady state catalysis in a manner that depends on ToMOC concentration. Through rapid kinetic assays, we demonstrate that ToMOD attenuates formation of the ToMOC−ToMOH complex. These data, coupled with protein docking studies, support a competitive model in which ToMOD and ToMOC compete for the same binding site on the hydroxylase. These results are discussed in the context of other studies of additional proteins in the superfamily of bacterial multicomponent monooxygenases.

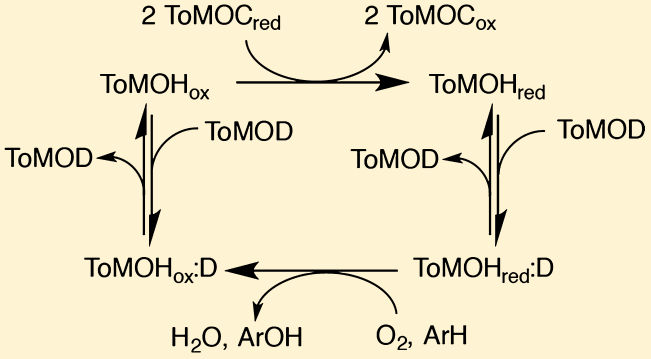

Bacterial multicomponent monooxygenases (BMMs) comprise a family of enzymes that can hydroxylate or epoxidize a variety of hydrocarbon substrates.[1] Enzyme systems in this superfamily contain either three or four component proteins that are necessary for catalysis. Included are (i) a catalytic hydroxylase housing two carboxylate-rich diiron active sites; (ii) a 12−16 kDa regulatory protein; (iii) an NADH oxidoreductase containing an NADH binding site, a flavin adenine dinucleotide, and a [2Fe-2S] ferredoxin cluster; and (iv) a Rieske protein that is present only in the four-component BMMs.[2] Protein interactions involving three-component BMMs have been thoroughly discussed in the literature.[3−5] Four-component BMMs are less well investigated and more complicated, because of their more extended electron transfer (ET) chain. In three-component BMMs, the NADH oxidoreductase directly reduces the diiron(III) centers in the hydroxylase, each by two electrons, without the need for additional proteins.[6−8] In contrast, the NADH oxidoreductase of four-component BMMs is incapable of directly reducing the hydroxylase.[9] Instead, this reduction is effected by the Rieske protein, designated ToMOC for the four-component BMM toluene/*o*-xylene monooxygenase (ToMO). Thus, either a ternary complex, involving the hydroxylase (ToMOH), ToMOC, and the NADH-oxidoreductase (ToMOF) proteins, must form, or sequential interactions between ToMOC and ToMOH may occur, as diagrammatically represented for the four-component BMM, ToMO, in Scheme 1. Scheme 1 intentionally omits any contribution from the regulatory protein, ToMOD.

Interactions of the regulatory protein with the hydroxylase have been thoroughly described for the four-component BMM

Scheme 1. Model for the Intermolecular Single-ET Events within the Four-Component BMM, Toluene/*o*-Xylene Monooxygenase (ToMO)

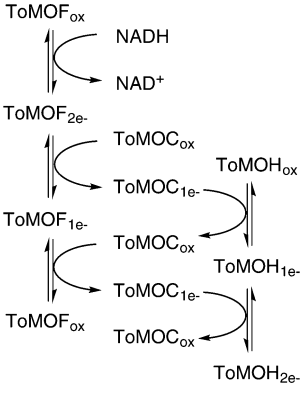

Received: May 21, 2014
Revised: October 28, 2014
Published: November 17, 2014

toluene 4-monooxygenase (T4MO) using both equilibrium binding measurements[10] and X-ray crystallography.[11,12] Reported functions of the regulatory protein include opening oxygen access to the diiron active site of the hydroxylase[13,14] and closing the entry point for an aromatic substrate within the hydroxylase.[11] The roles of the regulatory protein with respect to ET kinetics and the function of the ET proteins remain unexplored for four-component BMMs, however.[a] To address this issue, we carried out steady state and pre-steady state experiments with the four-component BMM ToMO from *Pseudomonas* sp. OX1. We find that excess ToMOD inhibits steady state turnover and that this inhibition is dependent on the concentration of ToMOC and the temperature of the reaction. ET studies demonstrate that the interaction between reduced ToMOC ($ToMOC_{red}$) and oxidized ToMOH ($ToMOH_{ox}$) is diminished in the presence of ToMOD. Finally, chemical cross-linking and protein docking studies support a competitive binding model, in which ToMOC and ToMOD compete for binding to the same region of ToMOH. These conclusions provide evidence for a dynamic interaction of ToMOH with both ToMOD and ToMOC. Possible functions for these interactions are discussed in the context of previous reports on three- and four-component BMMs.

EXPERIMENTAL PROCEDURES

General Methods. Plasmids for the component proteins of ToMO were generously provided by the Di Donato laboratory (Naples, Italy). Expression and purification of ToMOC, ToMOD, ToMOF, and ToMOH were carried out as reported previously.[15,16] NADH and *N*-[3-(dimethylamino)propyl]-*N*′-ethylcarbodiimide (EDC) were purchased from Roche and Sigma, respectively. ToMOH is an $(\alpha\beta\gamma)_2$ dimer, with carboxylate-bridged diiron centers contained in each α subunit. In this work, the concentration of ToMOH is represented as that of the $(\alpha\beta\gamma)_2$ dimer.

Steady State Kinetics and Analysis. Reactions were examined in 400 μL volumes of 0.1 M Tris buffer at pH 7.3. Each reaction mixture contained 2 μM ToMOH (4 μM diiron active sites), 0.5−120 μM ToMOD, 2−16 μM ToMOC, 0.1 μM ToMOF, and saturating levels of toluene (~6 mM).[17] Reactions were initiated by addition of NADH to a final concentration of 0.2 mM. The absorbance change at 340 nm, corresponding to conversion of NADH to NAD^+, was monitored as a function of time. The temperature was maintained at either 10 or 37 °C using a circulating water bath. The reaction cuvette was held in a thermostated compartment attached to a circulating water bath. The rate of NADH consumption was calculated by fitting the initial absorbance change at 340 nm to a linear function. The negative slope of this line was divided by both the extinction coefficient of NADH (6220 M^{-1} cm^{-1}) and the concentration of ToMOH diiron sites (4 μM) to yield the NADH consumption per diiron active site. The resulting values were plotted as a function of ToMOD concentration. Fits to the data were examined for a standard Michaelis−Menten model, a cooperative model, and a competitive model (eq 1).

$$\frac{v}{[\text{ToMOH diiron sites}]} = \frac{k_{cat}}{1 + \frac{K_m}{[\text{ToMOD}]} + \frac{[\text{ToMOD}]}{K_i}} \quad (1)$$

In all cases, ToMOD was treated as a substrate, a common method for evaluating promoter proteins.[18] The competitive model was clearly best as indicated by the lowest adjusted R^2, the lowest error of the fitted parameters, and residual values closest to zero.

Colorimetric Reductive Titrations. Anaerobic titrations were performed in sealed cuvettes in 50 mM potassium phosphate and 50 mM NaCl (pH 7.0) at 25 °C. In a nitrogen-filled chamber, solutions of 40−50 μM ToMOC and either 40 μM anthraquinone-1,5-sulfonic acid (E_m° = −175 mV vs NHE),[19] 100 μM 2-hydroxy-1,4-naphthoquinone (E_m° = −137 mV vs NHE),[20] or 17.5 μM indigo carmine (E_m° = −125 mV vs NHE)[21] were prepared. Each solution was sealed in a quartz cuvette with a screw cap equipped with a rubber septum. A buffered dithionite solution was loaded into a gastight Hamilton syringe with a repeating dispenser. The syringe and cuvette were removed from the anaerobic chamber, and each ToMOC/dye solution was titrated with the buffered solution of dithionite. An HP diode array spectrometer was used to monitor the UV−vis spectrum of the sample throughout the course of the titration. The solution was allowed to reach equilibrium, which was achieved when no further absorbance change was observed (5−30 min). The equilibrium absorbance spectrum for each titration point was fit to a linear combination of oxidized and reduced absorbance spectra of ToMOC and the dye (eq 2). The reduction potential of ToMOC was determined from a modified Nernst equation (eq 3)[22]

$$y = a \times \text{Abs}_{\text{ToMOC}_{ox}} + b \times \text{Abs}_{\text{ToMOC}_{red}} + c \times \text{Abs}_{\text{dye}_{ox}} + d \times \text{Abs}_{\text{dye}_{red}} \quad (2)$$

$$E = E^{\circ\prime}_{dye} - \frac{RT}{n_{dye}F}\ln\left(\frac{[\text{dye}_{red}]}{[\text{dye}_{ox}]}\right) = E^{\circ\prime}_{\text{ToMOC}} - \frac{RT}{bn_{\text{ToMOC}}F}\ln\left(\frac{[\text{ToMOC}_{red}]}{[\text{ToMOC}_{ox}]}\right) \quad (3)$$

where $E^{\circ\prime}_{dye}$ and $E^{\circ\prime}_{\text{ToMOC}}$ are the midpoint potentials of the dye and ToMOC, respectively; n_{dye} and n_{ToMOC} are the number of electrons that the components can acquire upon reduction; F is Faraday's constant; and E is the equilibrium midpoint potential of the solution.

Stopped-Flow Kinetics and Analysis for Single-Wavelength Measurements. Single-wavelength kinetic data were obtained using a Hi-Tech Scientific (Salisbury, U.K.) SF-61 DX2 stopped-flow spectrophotometer equipped with a photomultiplier tube and a tungsten lamp. To remove oxygen from the reaction lines, the instrument was scrubbed overnight with anaerobic buffer containing ~5 mM sodium dithionite. Immediately prior to each experiment, the stopped-flow lines were washed with dithionite-free, anaerobic buffer to remove any excess dithionite. Reactions were carried out in 50 mM potassium phosphate and 50 mM NaCl at pL 7.0. The pD was calculated by adding 0.4 to the value reported by the pH meter. The temperature was held constant using a circulating water bath. Temperatures for all stopped-flow reactions were 13 °C, except where noted otherwise. Protein samples were made anaerobic by cycling between vacuum and argon using a Schlenk line. The anaerobic protein samples were brought into a chamber filled with a nitrogen atmosphere for handling prior to stopped-flow analysis. In the nitrogen chamber, the two reactants were loaded into separate Hamilton Sample-Lock syringes equipped with a male luer adapter. The syringes were sealed and removed from the nitrogen atmosphere for loading onto the prewashed stopped-flow. Protein concentrations listed for stopped-flow experiments are concentrations after rapid mixing of the reaction components. Three or more individual traces were averaged to obtain the final traces shown here. The

dx.doi.org/10.1021/bi500892n | *Biochemistry* 2014, 53, 7368−7375

data were analyzed using OriginLabs 9.0 or 9.1. Single- and double-exponential fits were compared as models for each of the averaged traces.

For reactions between $ToMOC_{red}$ and $ToMOH_{ox}$, $ToMOC_{red}$ was prepared by titrating $ToMOC_{ox}$ with a buffered solution of dithionite under a nitrogen atmosphere. When the regulatory protein was included, ToMOD was added to the syringe containing either $ToMOH_{ox}$ or $ToMOC_{red}$. Using the stopped-flow, the absorbance change at 458 nm was monitored for each reaction condition. This wavelength provides the greatest difference in molar extinction coefficient for the oxidized and reduced forms of ToMOC. Single-exponential fits were adequate to fit all experimental traces. In some cases, double-exponential fits resulted in lower adjusted R^2 values. However, in all cases, double-exponential fits also produced greater errors of the fitted parameters. The error for double-exponential fits was greater than 10 times the output parameter. For this reason, double-exponential fits were not further considered.

Stopped-Flow Kinetics and Analysis for Multiwavelength Measurements. Multiwavelength kinetic data were obtained using a Hi-Tech Scientific SF-61 DX2 stopped-flow spectrophotometer equipped with a diode array detector and a xenon lamp. Anaerobic preparation of the stopped-flow was the same as indicated for single-wavelength measurements (above). Reactions were carried out in 50 mM potassium phosphate and 50 mM sodium chloride at pH 7.0 and 13 °C. Under a nitrogen atmosphere, reduced ToMOF ($ToMOF_{red}$) was prepared by adding 1.5 equiv of NADH. $ToMOC_{ox}$ and $ToMOF_{red}$ were loaded into separate Hamilton Sample-Lock syringes equipped with a male luer lock. Absorbance changes from 380 to 750 nm were monitored as a function of time. The reaction was very fast (complete in 15 ms), such that only the first three data points displayed a change in absorbance. Because of the speed of the reaction, the absorbance traces are shown and discussed but were not fit to a kinetic model.

Cross-Linking Experiments. A solution of 120 μM ToMOC or ToMOF and 60 μM ToMOH was prepared in 25 mM MOPS buffer at pH 7.0. For reaction mixtures containing the regulatory protein, ToMOD was added to a final concentration of 120 μM. The zero-atom cross-linking agent EDC was added to the protein solution to a final concentration of 450 mM. The reaction mixture was kept on ice for 1 h. An equal volume of 1 M sodium acetate and 25 mM MOPS at pH 6.8 was added after 1 h to quench the reaction. The products were loaded onto a Sephadex S200 column (1.6 cm × 60 cm). The protein was eluted with 25 mM MOPS (pH 7.0), 10% glycerol (v/v), and 150 mM NaCl. Fractions of 3 mL were collected throughout the elution. The fractions were analyzed by UV−vis spectroscopy. The absorbance at 280 and 458 nm was plotted as a function of elution volume.

RESULTS AND DISCUSSION

Effect of ToMOD and ToMOC Concentration on Steady State Activity. To assess the effects of ToMOD on catalysis, we performed steady state reactions with varying concentrations of ToMOD. Influenced by prior reports with three-component BMMs,[4] we assessed activity at both 10 and 37 °C (Figure 1).

At substoichiometric concentrations of ToMOD, the rate of NADH consumption increases with increasing ToMOD concentration at both 10 and 37 °C. Under these conditions, ToMOD acts as a promoter protein. X-ray crystallography

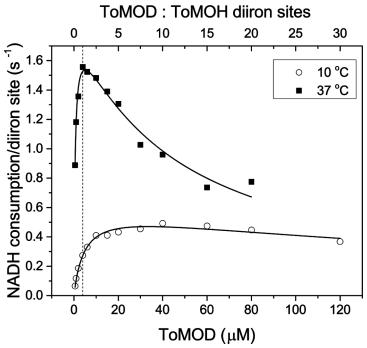

Figure 1. Steady state activity as a function of ToMOD concentration at 10 °C (○) and 37 °C (■). Reactions of 2 μM ToMOH, 4 μM ToMOC, 0.5−120 μM ToMOD, 0.1 μM ToMOF, and saturating amounts of toluene (~6 mM) were initiated by addition of 0.2 mM NADH. The rate of NADH consumption as a function of ToMOD concentration fit well to a ToMOD inhibition model (eq 1 of the Supporting Information). The vertical, dashed line in the figure demarcates a 1:1 ratio of ToMOD to ToMOH diiron sites.

indicates that promotion by ToMOD arises through conformational changes exerted on ToMOH upon binding of ToMOD. These conformational changes within the hydroxylase enable dioxygen access to the diiron active site and subsequent oxygen activation.[13,14] With excess ToMOD, however, we observed an inhibitory effect, $K_{i,ToMOD}$.[b] Importantly, ToMOD is much more effective at inhibiting the reaction at 37 °C than at 10 °C.

Similar steady state experiments were performed with varying concentrations of ToMOC (Figure 2 and Table 1).

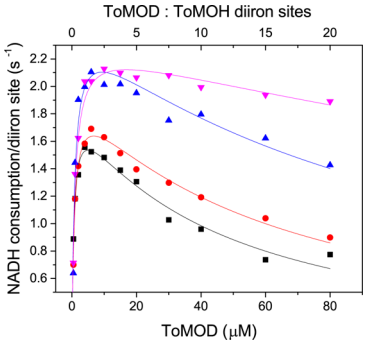

Figure 2. Steady state activity at various concentrations of ToMOC graphed as a function of ToMOD concentration. At 37 °C, the rate of NADH consumption as a function of ToMOD concentration was determined for varying concentrations of ToMOC, 4 μM (black squares), 8 μM (red circles), 10 μM (blue triangles), and 16 μM (pink inverted-triangles). Each reaction mixture contained 2 μM ToMOH, 0.1 μM ToMOF, saturating toluene, and 0.2 mM NADH.

Upon increasing the concentration of ToMOC, there are significant shifts in the apparent k_{cat}, $K_{m,ToMOD}$, and $K_{i,ToMOD}$ values, as numerically shown in Table 1. The most dramatic change is in the $K_{i,ToMOD}$, which reflects much weaker ToMOD

Table 1. Steady State Parameters

[ToMOC] (μM)	k_{cat} (s^{-1})	$K_{m,ToMOD}$ (μM)	$K_{i,ToMOD}$ (μM)
4	1.88(5)	0.57(6)	44(4)
6	2.00(5)	0.75(8)	60(5)
10	2.5(2)	0.8(1)	110(30)
16	2.34(6)	0.87(9)	330(50)

dx.doi.org/10.1021/bi500892n | Biochemistry 2014, 53, 7368−7375

inhibition at high concentrations of ToMOC. The dependence of $K_{i,ToMOD}$ on ToMOC concentration demonstrates that the inhibitory function of ToMOD is linked to the action of ToMOC.

X-ray crystallographic data indicate that binding of the T4MO regulatory protein to its hydroxylase covers the entrance to the aromatic substrate channel and shrinks its diameter.[11,12] Attenuation of substrate access may therefore also contribute to inhibition at the higher ToMOD concentrations. To assess this possibility directly, steady state experiments with varying concentrations of ToMOD were performed at 0.75 and 5 mM toluene (Figure 3).

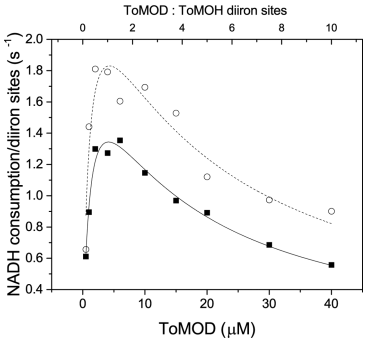

Figure 3. Turnover as a function of toluene and ToMOD concentrations. At 37 °C, the rate of NADH consumption as a function of ToMOD concentration was determined at 0.75 mM (■) and 5.0 mM (○) toluene. Each reaction mixture contained 2 μM ToMOH, 2 μM ToMOC, 0.1 μM ToMOF, toluene, and 0.2 mM NADH.

The $k_{cat,ToMOD}$ increases from 2.1(1) s^{-1} at 0.75 mM toluene to 2.7(4) s^{-1} at 5 mM toluene. In contrast, $K_{i,ToMOD}$ is unaltered, yielding values of 14(2) and 17(5) μM for 0.75 and 5 mM toluene, respectively. Thus, covering of the aromatic substrate channel by ToMOD does not affect $K_{i,ToMOD}$ under the conditions presented here. Instead, this inhibition constant depends directly on ToMOC concentration. The data provide further support for the model involving direct competition between ToMOC and ToMOD for binding to the hydroxylase. This result may arise either through competition for the same binding location or by one protein at the same site triggering allosteric changes that alter the conformation of ToMOH and affect the binding of the other protein at a remote site.

The sites of the interaction between BMM regulatory proteins and their respective hydroxylases are well documented.[11,12,23,24] The regulatory proteins bind to the hydroxylases in a region originally termed the "canyon" for the first BMM hydroxylase characterized by X-ray crystallography, sMMOH[25] from soluble methane monooxygenase (sMMO). Subsequent X-ray crystallography demonstrated that the canyon region occurs in all members of the BMM family.[12,23,26] The canyon is defined by a significant depression at the surface of these hydroxylases formed between α and β subunits across the dimer interface. The shortest distance between the diiron active sites and the surface of the hydroxylases, ∼12 Å, exits at one of the canyon walls, the locale of regulatory protein binding.[12,23,24] Although short distances are not required for biochemical ET,[27−29] binding of ToMOC to ToMOH in the canyon would provide the most efficient distance for ET.[30] If ToMOC were to bind in the canyon, which we consider to be quite likely for efficient ET, ToMOD would compete with ToMOC for binding to ToMOH.

Electron Transfer. To assess competition between ToMOD and ToMOC for binding to ToMOH, we evaluated intermolecular ET. Monitoring ET provides a direct assessment of inhibition without the need to unravel the complex kinetics of steady state turnover involving four protein components and multiple substrates. In these investigations, we examined the thermodynamic and kinetic parameters of ET from $ToMOC_{red}$ to ToMOH by exploiting redox-dependent absorbance features of ToMOC. Upon oxidation of $ToMOC_{red}$, the absorbance at 458 nm increases 2-fold (Supporting Information), allowing for kinetic characterization of ET to and from ToMOC as well as facile redox determination by colorimetric methods. The midpoint potential of ToMOC was determined by a colorimetric reductive titration to be −130(30) mV versus NHE (Supporting Information). This midpoint potential is near that reported for T4moC (−173 mV vs NHE)[31] and lies between those expected for the [2Fe-2S] cluster of ToMOF (−205 mV vs NHE at 25 °C)[32] and the diiron center in ToMOH (+48 mV vs NHE at 4 °C).[5] These results indicate that the Rieske cluster of ToMOC is thermodynamically suitable for shuttling electrons from the redox centers of ToMOF to the redox centers of ToMOH. ET from the reduced ToMOF to $ToMOC_{ox}$ is rapid (complete in <15 s) and much faster than steady state turnover (Supporting Information). Despite this limitation with respect to kinetic quantitation, these results demonstrate that ET between ToMOF and ToMOC is not rate-limiting along the ET pathway and that a ternary complex involving ToMOF, ToMOC, and ToMOH is not necessary for ET from ToMOF to ToMOC.

We next assessed ET to $ToMOH_{ox}$ from $ToMOC_{red}$ as monitored by stopped-flow UV−vis spectroscopy. The data were obtained using limiting concentrations of $ToMOC_{red}$, such that only a single electron would be transferred to the hydroxylase to form one-electron reduced, mixed-valent ToMOH ($ToMOH_{mv}$). Figure 4 shows the observed rate

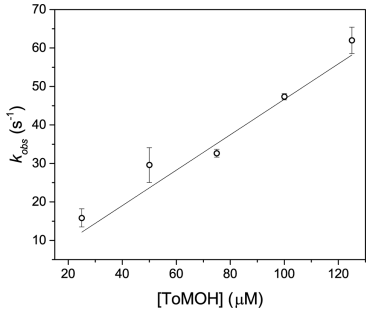

Figure 4. ET from $ToMOC_{red}$ to $ToMOH_{ox}$ as a function of ToMOH concentration. k_{obs} values for the reaction between 5 μM $ToMOC_{red}$ and varying concentrations of $ToMOH_{ox}$ at pH 7.0 and 13 °C. The data fit well to a linear function with a slope of 0.42(5) μM^{-1} s^{-1}.

constants derived from single-exponential fits of the absorbance change at 458 nm. At excess ToMOH, the observed rate constant depends linearly upon the concentration of ToMOH, from which a second-order rate constant of 0.42(5) μM^{-1} s^{-1} could be derived (Figure 4), consistent with a bimolecular reaction between the two proteins. The observed absorbance change corresponded to complete oxidation of $ToMOC_{red}$. At ToMOH concentrations of ≥200 μM, the solution viscosity began to affect the instrument mixing time, and it was not

dx.doi.org/10.1021/bi500892n | Biochemistry 2014, 53, 7368−7375

possible to obtain meaningful results in this range. These data do not permit the evaluation of the true ET reaction (see the Supporting Information for more complete studies). The role of ToMOD in this reaction is discussed in the following section.

Effect of ToMOD on ET. With the use of pre-steady state single-mixing stopped-flow experiments, we examined the effect of increasing concentrations of ToMOD, premixed with $ToMOH_{ox}$, on electron transfer from $ToMOC_{red}$. Under these conditions, the observed rate constant for ET decreased significantly as the concentration of ToMOD increased. Figure 5 shows the average absorbance change at increasing

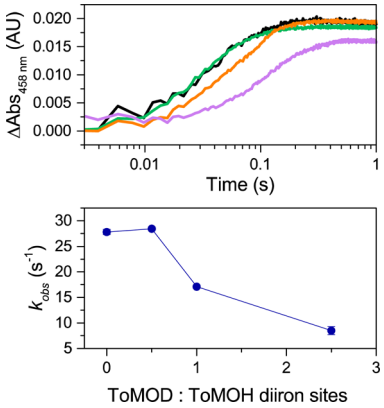

Figure 5. ET from $ToMOC_{red}$ to $ToMOH_{ox}$ preincubated with ToMOD. The absorbance at 458 nm was monitored for the reaction between $ToMOC_{red}$ and $ToMOH_{ox}$ preincubated with 0 μM (black), 25 μM (green), 50 μM (orange), and 125 μM (violet) ToMOD. The absorbance change at 458 nm over time is plotted on a logarithmic scale (top), and the observed rate constants obtained from single-exponential fits of the data are shown as a function of the ratio of ToMOD to ToMOH diiron sites (bottom).

concentrations of ToMOD. A control experiment revealed that preincubation of ToMOD with $ToMOC_{red}$ did not change the results from those obtained in the absence of ToMOD (Supporting Information, Figure S6). Thus, ToMOD slows the reaction between $ToMOC_{red}$ and $ToMOH_{ox}$ through its interaction with ToMOH. An inhibitory effect upon ET could be a consequence of competitive binding, noncooperative allosteric effects including conformational changes, or an alteration of the ToMOH redox potential in the presence of ToMOD. The last possibility is suggested by the finding that, for the three-component BMM soluble methane monooxygenase (sMMO), addition of the regulatory protein to the hydroxylase shifts the redox potential to a more negative value.[5] Thus, alteration of the redox potential of ToMOH by ToMOD binding would not be unprecedented. Attenuation of the redox potential of ToMOH by ToMOD, however, would not give rise to a $K_{i,ToMOD}$ that depends on ToMOC concentration, as we report here on the basis of steady state data. Therefore, we propose either that ToMOD and ToMOC compete for binding to the same location on ToMOH or that ToMOD enforces allosteric effects on ToMOH, inhibiting ET from $ToMOC_{red}$ to $ToMOH_{ox}$ throughout turnover.

Binding Interactions. To verify further that ToMOC and ToMOH interact and that this interaction is perturbed by ToMOD, we studied the binding of these proteins by use of the zero-atom cross-linking agent EDC. The cross-linking reaction was analyzed by gel chromatography to separate the products by size without denaturation. Absorbance measurements (Figure 6) were obtained for isolated fractions from the

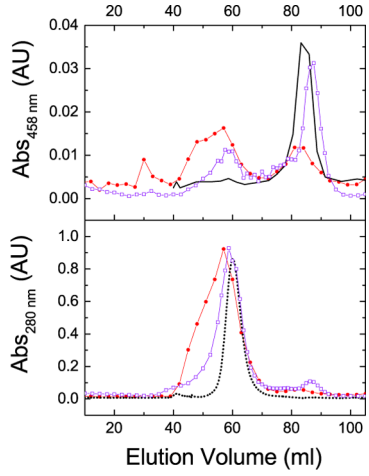

Figure 6. Cross-linking of ToMOC and ToMOH in the presence and absence of ToMOD. Values of absorbance at 458 nm (top) and 280 nm (bottom) as a function of elution volume are shown. Elution of ToMOC alone is shown with a solid black line; elution of ToMOH alone is shown with a dotted black line. Elution of the reaction mixture of ToMOC, ToMOH, and the cross-linking agent EDC is shown as a red trace with red dots. Elution of the reaction mixture of ToMOC, ToMOH, ToMOD, and the cross-linking agent EDC is shown as a purple trace with empty squares. Absorbance measurements at 458 nm were performed for each fraction, whereas absorbance measurements at 280 nm were an output from the Äkta fast protein liquid chromatography system.

column flow-through. The absorbance at 458 nm was used as a way to determine the ToMOC retention time. The elution volumes for ToMOC and ToMOH alone are 80 and 60 mL, respectively (Figure 6, black traces). When ToMOC and ToMOH were incubated with EDC, the elution point of ToMOC shifted to 55 mL, overlapping with the peak of ToMOH alone (Figure 6, red traces). The reduction of retention time demonstrates that cross-linking of the two proteins increases the hydrodynamic radius of both ToMOH and ToMOC, showing that the two proteins bind in solution. In the presence of ToMOD, the absorption intensity at 458 nm was much stronger in the low-molecular weight fraction than in the high-molecular weight fraction. This result indicates that cross-linking of ToMOC and ToMOH is less efficient in the presence of ToMOD (Figure 6, purple traces), consistent with competition between ToMOD and ToMOC for a binding site on ToMOH. This result cannot distinguish between allosteric and direct competition for such a location.

ToMOF, on the other hand, did not cross-link with ToMOH under the same reaction conditions (Supporting Information). This result demonstrates that ToMOF would be incapable of transferring electrons to ToMOH because the two proteins cannot bind one another, a conclusion that is supported by the fact that there is no steady state activity in the ToMO system in the absence of ToMOC.[9]

Finally, to distinguish between direct competition and indirect allosteric inhibition, we used a computational approach involving an automated protein docking program.[33−35] Guided by X-ray crystal structure information,[12,26,36,37] we examined binding between T4moC and either ToMOH, T4moH, or the T4moHD complex.[c] The T4MO proteins used for this docking

dx.doi.org/10.1021/bi500892n | Biochemistry 2014, 53, 7368−7375

model are highly homologous with ToMO, display similar chemistry,[9,38] and have known structures from X-ray crystallography.[10−12] When T4moC was docked to either hydroxylase alone, the preferred binding site was conclusively at the canyon regions of the proteins (Figure 7A). This binding

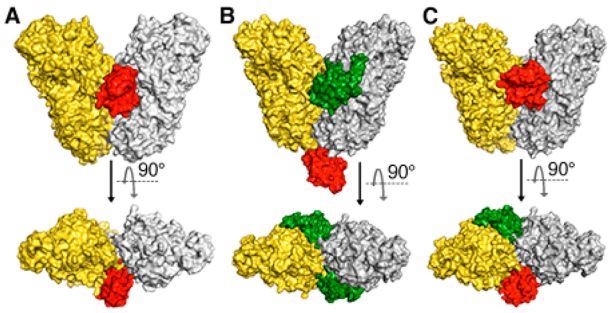

Figure 7. Binding predictions for T4moC and ToMO and the complex of T4moH with the regulatory protein. Shown above are representative models for the predicted binding interactions between T4moC and (A) ToMOH, (B) the complex of 2 equiv of the regulatory protein and the hydroxylase of T4moH, and (C) the complex of 1 equiv of the regulatory protein and the hydroxylase of T4MO. The hydroxylases are represented in surface mode with the two halves of the dimer colored yellow and gray. T4moC and the regulatory protein are colored red and green, respectively.

mode was similar for all 10 of the lowest-energy predictions (Chart S1 of the Supporting Information). When the T4moHD complex was used, the best predicted T4moC binding site was nonsensical for efficient ET (Figure 7B), being far removed from the hydroxylase diiron center, and not conserved among the 10 lowest-energy structures provided by the docking model (Chart S2 of the Supporting Information). Upon removal of one of the two regulatory proteins from the hydroxylase complex, T4moC bound to the canyon region on the side of T4moH from which ToMOD was removed (Figure 7C). In this case, the 10 lowest-energy structures all revealed binding of T4moC in a canyon region of the hydroxylase (Chart S3 of the Supporting Information). Use of the docking program necessitated removal of the 2Fe-2S Rieske cluster (see page 1 of the Supporting Information), which limits our ability to compute a distance for ET. The model nonetheless is consistent with a competitive binding model supported by ET and steady state turnover presented here and a recent X-ray crystal structure.[a]

Comparison of Three- and Four-Component BMMs: Conserved Control of Electron Transfer. The BMM regulatory proteins have been shown (i) to couple NADH consumption with hydrocarbon oxidation,[39] (ii) to gate hydrocarbon substrate[11] and dioxygen[13,14] access to the diiron active sites, and (iii) to alter the redox potential of the catalytic diiron active site.[5,40] Competition between the reductase and regulatory protein of the three-component BMM, sMMO, has been described in detail.[3,4,41] Recent studies of soluble butane monooxygenase (sBMO) also reveal a dual promotion and inhibition effect of the regulatory protein on turnover.[42] Because the Rieske protein of the four-component BMMs is much smaller than the NADH oxidoreductase of three-component BMMs, the Rieske protein might bind to the hydroxylase in a ternary complex with the regulatory protein. The present results, however, indicate that competitive binding between the electron transfer partner of the hydroxylase and the regulatory proteins is retained even in four-component BMMs. Additional evidence for competitive binding is available (see footnote [a]), which agrees with our conclusions. Conservation of this competition in both three- and four-component BMMs reveals that nature has preserved this mechanism despite radically altering the ET partners, suggesting that this feature of catalysis is indispensible. Competitive binding between the ET and regulatory proteins may provide a mechanism for controlling unwanted ET during dioxygen activation protecting the oxygen-activated intermediates from unwanted reduction.[3,41,43]

■ ASSOCIATED CONTENT

Supporting Information

Absorbance traces of ToMOC, colorimetric reductive titrations with fits, absorbance traces for the reactions between $ToMOC_{red}$ and $ToMOH_{ox}$, and output for the automated protein docking models. This material is available free of charge via the Internet at http://pubs.acs.org.

■ AUTHOR INFORMATION

Corresponding Author

*E-mail: lippard@mit.edu. Telephone: (617) 253-1892.

Funding

This work was funded by the National Institute of General Medical Sciences via Grant 5-R01-GM032134. A.D.L. thanks the National Institutes of Health for partial support under Interdepartmental Biotechnology Training Grant T32 GM008334.

Notes

The authors declare no competing financial interest.

■ ACKNOWLEDGMENTS

We thank Woon Ju Song and Kanchana Ravichandran for helpful discussions.

■ ABBREVIATIONS

ToMO, toluene/*o*-xylene monooxygenase; BMM, bacterial multicomponent monooxygenase; NADH, nicotinamide adenine dinucleotide; ET, electron transfer; T4MO, toluene 4-monooxygenase; ToMOD, regulatory protein of ToMO; ToMOC, Rieske protein of ToMO; ToMOH, hydroxylase of ToMO; ToMOF, NADH oxidoreductase of ToMO; EDC, *N*-[3-(dimethylamino)propyl]-*N*′-ethylcarbodiimide; $ToMOC_{red}$, one-electron-reduced Rieske protein of ToMO; $ToMOH_{ox}$, oxidized hydroxylase of ToMO; $ToMOF_{red}$, two- or three-electron-reduced NADH oxidoreductase of ToMO; $ToMOC_{ox}$, oxidized Rieske protein of ToMO; NHE, normal hydrogen electrode; $ToMOH_{mv}$, one-electron-reduced hydroxylase of ToMO; $ToMOH_{red}$, two-electron-reduced hydroxylase of ToMO; sMMO, soluble methane monooxygenase.

■ ADDITIONAL NOTES

[a]While this paper was in revision, a related study of T4MO appeared,[43] to which we draw the reader's attention. These structural studies for T4MO are consistent with the results and conclusions presented here.

[b]The ratio of ToMOC to diiron sites in ToMOH is 1:1 for the data in Figure 1. At this ratio, maximal NADH consumption occurs at a 1:1 ratio of ToMOD to ToMOH diiron sites, which was the first indication of binding competition or allostery during steady state catalysis.

[c]The Rieske, regulatory, and hydroxylase proteins of T4MO are designated T4moC, T4moD, and T4moH, respectively. The complex of T4moH with two regulatory proteins is termed T4moHD.

REFERENCES

(1) Notomista, E., Lahm, A., Di Donato, A., and Tramontano, A. (2003) Evolution of Bacterial and Archaeal Multicomponent Monooxygenases. *J. Mol. Evol. 56*, 435−445.

(2) Leahy, J. G., Batchelor, P. J., and Morcomb, S. M. (2003) Evolution of the Soluble Diiron Monooxygenases. *FEMS Microbiol. Rev. 27*, 449−479.

(3) Fox, B. G., Liu, Y., Dege, J. E., and Lipscomb, J. D. (1991) Complex Formation between the Protein Components of Methane Monooxygenase from *Methylosinus trichosporium* OB3b: Identification of Sites of Component Interaction. *J. Biol. Chem. 266*, 540−550.

(4) Gassner, G. T., and Lippard, S. J. (1999) Component Interactions in the Soluble Methane Monooxygenase System from *Methylococcus capsulatus* (Bath). *Biochemistry 38*, 12768−12785.

(5) Paulsen, K. E., Liu, Y., Fox, B. G., Lipscomb, J. D., Münck, E., and Stankovich, M. T. (1994) Oxidation-Reduction Potentials of the Methane Monooxygenase Hydroxylase Component from *Methylosinus trichosporium* OB3b. *Biochemistry 33*, 713−722.

(6) Blazyk, J. L., Gassner, G. T., and Lippard, S. J. (2005) Intermolecular Electron-Transfer Reactions in Soluble Methane Monooxygenase: A Role for Hysteresis in Protein Function. *J. Am. Chem. Soc. 127*, 17364−17376.

(7) Fox, B. G., Hendrich, M. P., Surerus, K. K., Andersson, K. K., Froland, W. A., Lipscomb, J. D., and Münck, E. (1993) Mössbauer, EPR, and ENDOR Studies of the Hydroxylase and Reductase Components of Methane Monooxygenase from *Methylosinus trichosporium* Ob3b. *J. Am. Chem. Soc. 115*, 3688−3701.

(8) Lund, J., Woodland, M. P., and Dalton, H. (1985) Electron-Transfer Reactions in the Soluble Methane Monooxygenase of *Methylococcus capsulatus* (Bath). *Eur. J. Biochem. 147*, 297−305.

(9) Cafaro, V., Scognamiglio, R., Viggiani, A., Izzo, V., Passaro, I., Notomista, E., Dal Piaz, F., Amoresano, A., Casbarra, A., Pucci, P., and Di Donato, A. (2002) Expression and Purification of the Recombinant Subunits of Toluene/*o*-Xylene Monooxygenase and Reconstitution of the Active Complex. *Eur. J. Biochem. 269*, 5689−5699.

(10) Moe, L. A., McMartin, L. A., and Fox, B. G. (2006) Component Interactions and Implications for Complex Formation in the Multicomponent Toluene 4-Monooxygenase. *Biochemistry 45*, 5478−5485.

(11) Bailey, L. J., Acheson, J. F., McCoy, J. G., Elsen, N. L., Phillips, G. N., and Fox, B. G. (2012) Crystallographic Analysis of Active Site Contributions to Regiospecificity in the Diiron Enzyme Toluene 4-Monooxygenase. *Biochemistry 51*, 1101−1113.

(12) Bailey, L. J., McCoy, J. G., Phillips, G. N., and Fox, B. G. (2008) Structural Consequences of Effector Protein Complex Formation in a Diiron Hydroxylase. *Proc. Natl. Acad. Sci. U.S.A. 105*, 19194−19198.

(13) McCormick, M. S., and Lippard, S. J. (2011) Analysis of Substrate Access to Active Sites in Bacterial Multicomponent Monooxygenase Hydroxylases: X-ray Crystal Structure of Xenon-Pressurized Phenol Hydroxylase from *Pseudomonas sp.* OX1. *Biochemistry 50*, 573−573.

(14) Song, W. J., Gucinski, G., Sazinsky, M. H., and Lippard, S. J. (2011) Tracking a Defined Route for O_2 Migration in a Dioxygen-Activating Diiron Enzyme. *Proc. Natl. Acad. Sci. U.S.A. 108*, 14795−14800.

(15) Liang, A. D., Wrobel, A. T., and Lippard, S. J. (2014) A Flexible Glutamine Regulates the Catalytic Activity of Toluene *o*-Xylene Monooxygenase. *Biochemistry 53*, 3585−3592.

(16) Song, W. J., Behan, R. K., Naik, S. G., Huynh, B. H., and Lippard, S. J. (2009) Characterization of a Peroxodiiron(III) Intermediate in the T201S Variant of Toluene/*o*-Xylene Monooxygenase Hydroxylase from *Pseudomonas* sp. OX1. *J. Am. Chem. Soc. 131*, 6074−6075.

(17) Yalkowsky, S. H., He, Y., and Jain, P. (2010) *Handbook of aqueous solubility data*, 2nd ed., CRC Press, Boca Raton, FL.

(18) Cook, P. F., and Cleland, W. W. (2007) *Enzyme Kinetics and Mechanism*, Garland Science, London.

(19) Fultz, M. L., and Durst, R. A. (1982) Mediator Compounds for the Electrochemical Study of Biological Redox Systems: A Compilation. *Anal. Chim. Acta 140*, 1−18.

(20) Nedbal, L., Samson, G., and Whitmarsh, J. (1992) Redox State of a One-Electron Component Controls the Rate of Photoinhibition of Photosystem II. *Proc. Natl. Acad. Sci. U.S.A. 89*, 7929−7933.

(21) Kettle, A. J., Clark, B. M., and Winterbourn, C. C. (2004) Superoxide Converts Indigo Carmine to Isatin Sulfonic Acid: Implications for the Hypothesis that Neutrophils Produce Ozone. *J. Biol. Chem. 279*, 18521−18525.

(22) Kopp, D. A., Gassner, G. T., Blazyk, J. L., and Lippard, S. J. (2001) Electron-Transfer Reactions of the Reductase Component of Soluble Methane Monooxygenase from *Methylococcus capsulatus* (Bath). *Biochemistry 40*, 14932−14941.

(23) Sazinsky, M. H., Dunten, P. W., McCormick, M. S., DiDonato, A., and Lippard, S. J. (2006) X-ray Structure of a Hydroxylase-Regulatory Protein Complex from a Hydrocarbon-Oxidizing Multicomponent Monooxygenase *Pseudomonas* sp. OX1 Phenol Hydroxylase. *Biochemistry 45*, 15392−15404.

(24) Lee, S. J., McCormick, M. S., Lippard, S. J., and Cho, U.-S. (2013) Control of Substrate Access to the Active Site in Methane Monooxygenase. *Nature 494*, 380−384.

(25) Rosenzweig, A. C., Frederick, C. A., Lippard, S. J., and Nordlund, P. (1993) Crystal Structure of a Bacterial Non-Haem Iron Hydroxylase That Catalyzes the Biological Oxidation of Methane. *Nature 366*, 537−543.

(26) Sazinsky, M. H., Bard, J., Di Donato, A., and Lippard, S. J. (2004) Crystal Structure of the Toluene/o-Xylene Monooxygenase Hydroxylase from *Pseudomonas stutzeri* OX1: Insight Into the Substrate Specificity, Substrate Channeling, and Active Site Tuning of Multicomponent Monooxygenases. *J. Biol. Chem. 279*, 30600−30610.

(27) Moser, C. C., Keske, J. M., Warncke, K., Farid, R. S., and Dutton, P. L. (1992) Nature of Biological Electron-Transfer. *Nature 355*, 796−802.

(28) Nordlund, N., and Reichard, P. (2006) Ribonucleotide Reductases. *Annu. Rev. Biochem. 75*, 681−706.

(29) Uhlin, U., and Eklund, H. (1994) Structure of Ribonucleotide Reductase Protein R1. *Nature 370*, 533−539.

(30) Lippard, S. J., and Berg, J. M. (1994) *Principles of Bioinorganic Chemistry*, University Science Books, Mill Valley, CA.

(31) Elsen, N. L., Moe, L. A., McMartin, L. A., and Fox, B. G. (2007) Redox and Functional Analysis of the Rieske Ferredoxin Component of the Toluene 4-Monooxygenase. *Biochemistry 46*, 976−986.

(32) Blazyk, J. L., and Lippard, S. J. (2002) Expression and Characterization of Ferredoxin and Flavin Adenine Dinucleotide Binding Domains of the Reductase Component of Soluble Methane Monooxygenase from *Methylococcus capsulatus* (Bath). *Biochemistry 41*, 15780−15794.

(33) Comeau, S. R., Gatchell, D. W., Vajda, S., and Camacho, C. J. (2004) ClusPro: A Fully Automated Algorithm for Protein-Protein Docking. *Nucleic Acids Res. 32*, W96−W99.

(34) Comeau, S. R., Gatchell, D. W., Vajda, S., and Camacho, C. J. (2004) ClusPro: An Automated Docking and Discrimination Method for the Prediction of Protein Complexes. *Bioinformatics 20*, 45−50.

(35) Kozakov, D., Brenke, R., Comeau, S. R., and Vajda, S. (2006) PIPER: An FFT-Based Protein Docking Program with Pairwise Potentials. *Proteins: Struct., Funct., Bioinf. 65*, 392−406.

(36) McCormick, M. S., Sazinsky, M. H., Condon, K. L., and Lippard, S. J. (2006) X-ray Crystal Structures of Manganese(II)-Reconstituted and Native Toluene/o-Xylene Monooxygenase Hydroxylase Reveal Rotamer Shifts in Conserved Residues and an Enhanced View of the Protein Interior. *J. Am. Chem. Soc. 128*, 15108−15110.

(37) Moe, L. A., Bingman, C. A., Wesenberg, G. E., Phillips, G. N., Jr., and Fox, B. G. (2006) Structure of T4moC, the Rieske-Type

Ferredoxin Component of Toluene 4-Monooxygenase. *Acta Crystallogr. D62*, 476−482.
(38) Pikus, J. D., Studts, J. M., Achim, C., Kauffmann, K. E., Münck, E., Steffan, R. J., McClay, K., and Fox, B. G. (1996) Recombinant Toluene-4-Monooxygenase: Catalytic and Mössbauer Studies of the Purified Diiron and Rieske Components of a Four-Protein Complex. *Biochemistry 35*, 9106−9119.
(39) Merkx, M., Kopp, D. A., Sazinsky, M. H., Blazyk, J. L., Müller, J., and Lippard, S. J. (2001) Dioxygen Activation and Methane Hydroxylation by Soluble Methane Monooxygenase: A Tale of Two Irons and Three Proteins. *Angew. Chem., Int. Ed. 40*, 2782−2807.
(40) Liu, K. E., and Lippard, S. J. (1991) Redox Properties of the Hydroxylase Component of Methane Monooxygenase from *Methylococcus capsulatus* (Bath): Effects of Protein-B, Reductase, and Substrate. *J. Biol. Chem. 266*, 12836−12839.
(41) Wang, W. X., Iacob, R. E., Luoh, R. P., Engen, J. R., and Lippard, S. J. (2014) Electron Transfer Control in Soluble Methane Monooxygenase. *J. Am. Chem. Soc. 136*, 9754−9762.
(42) Cooley, R. B., Dubbels, B. L., Sayavedra-Soto, L. A., Bottomley, P. J., and Arp, D. J. (2009) Kinetic Characterization of the Soluble Butane Monooxygenase from *Thauera butanivorans*, formerly '*Pseudomonas butanovora*'. *Microbiology 155*, 2086−2096.
(43) Acheson, J. F., Bailey, L. J., Elsen, N. L., and Fox, B. G. (2014) Structural Basis for Biomolecular Recognition in Overlapping Binding Sites in a Diiron Enzyme System. *Nat. Commun. 5*, DOI: 10.1038/ncomms6009.